ACS APPLIED MATERIALS & INTERFACES

Research Article

Cite This: ACS Appl. Mater. Interfaces 2019, 11, 10922−10932

www.acsami.org

Ultrasensitive and Highly Compressible Piezoresistive Sensor Based on Polyurethane Sponge Coated with a Cracked Cellulose Nanofibril/Silver Nanowire Layer

Shuaidi Zhang,[†] Hu Liu,[*,†,‡] Shuaiyuan Yang,[†] Xianzhang Shi,[†] Dianbo Zhang,[†] Chongxin Shan,[§] Liwei Mi,[∥] Chuntai Liu,[†] Changyu Shen,[†] and Zhanhu Guo[‡]

[†]Key Laboratory of Materials Processing and Mold (Zhengzhou University), Ministry of Education; National Engineering Research Center for Advanced Polymer Processing Technology, Zhengzhou University, Zhengzhou 450002, China

[‡]Integrated Composites Laboratory (ICL), Department of Chemical & Biomolecular Engineering, University of Tennessee, Knoxville, Tennessee 37996, United States

[§]School of Physics and Engineering, Zhengzhou University, Zhengzhou, Henan 450052, China

[∥]Center for Advanced Materials Research, Zhongyuan University of Technology, Zhengzhou, Henan 450007, China

Supporting Information

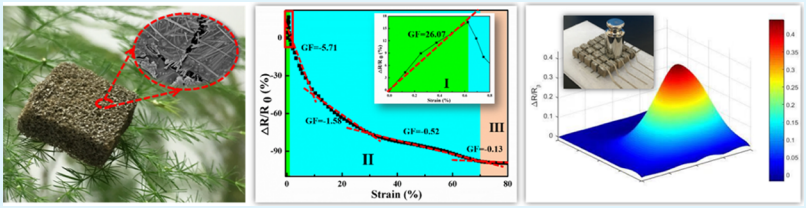

ABSTRACT: With the rapid development of flexible wearable electronics, a piezoresistive sensor with low detection limit and wide strain sensing range turns out to be a great challenge for its application in this field. Here, a cracked cellulose nanofibril/silver nanowire (CA) layer-coated polyurethane (PU) sponge was acquired through a simple dip-coating process followed by precompression treatment. The electrical conductivity and mechanical property of the conductive CA@PU sponge could be effectively tuned through changing the dip-coating number. As a piezoresistive sensor, the sponge exhibited the capability of detecting both small and large motions over a wide compression strain range of 0−80%. Based on the "crack effect", the sensor possessed a detection limit as low as 0.2% and the gauge factor [GF, GF = $(\Delta R/R_0)/\varepsilon$, where ΔR, R_0, and ε represent the instantaneous resistance change, original resistance, and strain applied, respectively] was as high as 26.07 in the strain range of 0−0.6%. Moreover, the "contact effect" enabled the sensor to be applicable for larger strain, and the GF decreased first and then became stable with increasing compression strain. In addition, frequency- and strain-dependent sensing performances were observed, demonstrating that the sensor can respond reliably to different applied frequencies and strains. Furthermore, the sensor displayed exceptional stability, repeatability, and durability over 500 cycles. Finally, the sensor could be applicable for the detection of various human bodily motions, such as phonation, stamping, knee bending, and wrist bending. Most importantly, the sponge also exhibited great potential for the fabrication of artificial electronic skin. Herein, the conductive CA@PU sponge will undoubtedly promote the development of high-performance flexible wearable electronics.

KEYWORDS: *PU sponge, silver nanowire, crack, ultrasensitive, piezoresistive sensor*

1. INTRODUCTION

Owing to the drawbacks (e.g., limited strain detection range, rigidity, and complex fabrication process) of conventional metal[1] and inorganic semiconductor[2] based sensors, high-performance flexible sensors have become a research hotspot with the rapid increase of flexible electronic industry, especially in the fields of electronic skin,[3−8] human−machine interfaces,[9−13] human health monitoring,[14−19] speech recognition systems,[20−24] and so forth. Currently, a variety of pressure sensors were designed according to different sensing mechanisms, including capacitive sensing,[25−28] piezoelectric sensing,[29−34] triboelectric sensing,[35] and resistive sensing.[36−40] Among them, a piezoresistive sensor, which converts external compressive pressure or strain into electrical resistance variation signal, has received great attentions because of its advantages of easy processing, simple structure, and low cost.[31,32]

An electrical conductive polymer nanocomposite (ECPC), obtained from the combination of electrical conductive filler with a polymer matrix through suitable processing technology, has turned out to be intriguing candidates for a high-performance piezoresistive sensor.[41−47] Its working principle

Received: January 15, 2019
Accepted: February 22, 2019
Published: February 22, 2019

DOI: 10.1021/acsami.9b00900
ACS Appl. Mater. Interfaces 2019, 11, 10922−10932

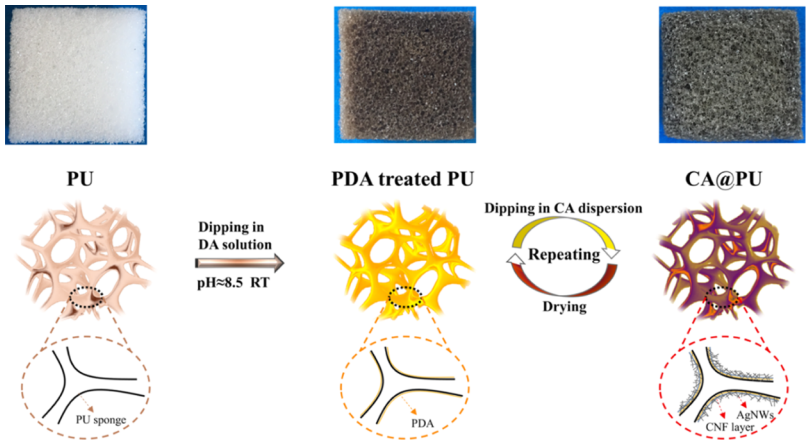

Figure 1. Schematic illustration for the preparation of conductive CA@PU sponge.

is mainly based on the deformation of ECPCs that induced the rearrangement of the conductive network upon external compressive pressure or strain, causing the variation of electrical resistance.[48−50] Especially, lightweight porous ECPC-based piezoresistive sensors provided an effective solution for the defect of small-strain detection range of conventional ones. Because of the high porosity and good elasticity of the polymer matrix, the "contact effect" between adjacent porous skeletons generated significant resistance variation signal over a wide strain range.[31,51,52] Recently, our group has successfully fabricated porous carbon nanotube/thermoplastic polyurethane (TPU)[53] and graphene/TPU[51] nanocomposites using the environment-friendly freeze-drying technique, displaying excellent piezoresistive sensing behaviors with excellent reproductivity and recoverability over 90% compression strain. In addition, commercial sponges were also proved to be an ideal substrate to prepare porous piezoresistive sensor through a simple dip-coating technique.[54,55] For instance, porous sea sponge was immersed into graphene and silver nanowire (AgNW) hybrid suspension, leaving conductive layer on the sponge skeleton after drying.[56] The as-prepared piezoresistive sensor exhibited high sensitivity over a detection range of 50% compression strain. However, the "contact effect" usually occurred under higher strain for these porous ECPCs discussed above, resulting a bad detectability toward small strain and limiting their special applications, such as artificial skin.

To obtain porous ECPCs with good detectability for both small and large strains simultaneously, a rational microstructure design appeared to be an effective method for fabricating innovative porous ECPC-based piezoresistive sensors.[57,58] Recently, ECPCs with a special microcrack structure have shown a very positive role for enhancing their sensitivity and detectability in the small-strain region based on the open and closure of the cracks.[57] For example, Wu et al. adopted an ion sputtering technique to fabricate conductive gold-coated PU sponge, and tunable crack densities were acquired through different precompression strains.[52] As a result, the conductive sponge possessed a low detection limit (0.5% strain), wide sensing range (55% strain), and good reproductivity. Meanwhile, graphene-coated PU sponge with a fractured fiber network was obtained through the hydrothermal treatment and precompression process, and a low-pressure detection limit of 9 Pa was successfully achieved.[59] However, the preparation processes of the samples stated above are complicated, which severely limit their large-scale production as piezoresistive sensors.

In this study, conductive cellulose nanofibril (CNF)/AgNWs (CA)-coated PU (CA@PU) sponge was fabricated using a simple dip-coating technique. Based on the high modulus of cellulose,[60] the brittle conductive CA layer was easy to be fractured upon external compression, constructing a cracked structure easily. In addition, the application of CNF was also beneficial for the dispersion of AgNWs and the good adhesion between the conductive layer and PU skeleton. The microstructure of the conductive CA@PU sponge was investigated using a scanning electron microscope (SEM), and the compression mechanical properties were also studied. Most importantly, the piezoresistive sensing performance of the conductive CA@PU sponge under small and large compression strains was systematically tested to verify its detection limit and sensing range. Finally, the piezoresistive sensor was applied to detect human bodily motion with different strains, and a CA@PU artificial electronic skin was also designed to illustrate its broad application prospect.

2. EXPERIMENTAL SECTION

2.1. Materials. Commercial PU sponge with a density of 25 kg/m^3 was purchased from Jiangxi Hongsiyuan Special Foam Material Co., Ltd. CNF aqueous dispersion with a solid content of 1 wt % was bought from Guilin Qihong Technology Co., Ltd. Dopamine hydrochloride (DA) and *tris*(hydroxymethyl-amino-methane) (Tris) were purchased from Shanghai Macklin Biochemical Co., Ltd. Silver nitrate ($AgNO_3$) was purchased from Sinopharm Chemical Reagent Co., Ltd China. Poly(vinylpyrrolidone) (PVP, M_w = 1 300 000 g mol^{-1}) was obtained from Usolf Chemical Technology Co., Ltd, Tsingtao, China. Sodium chloride (NaCl) was bought from Zhiyuan Reagent Co., Ltd, Tianjin, China. Ethylene glycol (EG), ethyl alcohol, and acetone were supplied by Tianjin Fuyu Fine Chemical Co., Ltd, Tianjin, China. All of the materials and chemicals were used as received.

2.2. Preparation of AgNWs. AgNWs used in this experiment were synthesized through a modified polyol procedure.[61,62] Briefly, 60 mL of PVP/EG solution (0.18 mol/L) and 30 μL of NaCl aqueous solution (0.1 mol/L) were first added into a three-necked flask and preheated at 170 °C in an oil bath for 90 min under stirring. Subsequently, 30 mL of freshly prepared $AgNO_3$/EG solution (0.12 mol/L) was added dropwise to the three-necked flask under stirring and heated at 170 °C for another 2.5 h. After reaction, the solution turned to be gray with a silky texture and cooled to room temperature. Then, the solution was added with a large amount of acetone and centrifuged (5000 rpm/min, 10 min) three times to purify the AgNWs. Finally, AgNWs were washed with ethanol three times to

DOI: 10.1021/acsami.9b00900
ACS Appl. Mater. Interfaces 2019, 11, 10922−10932

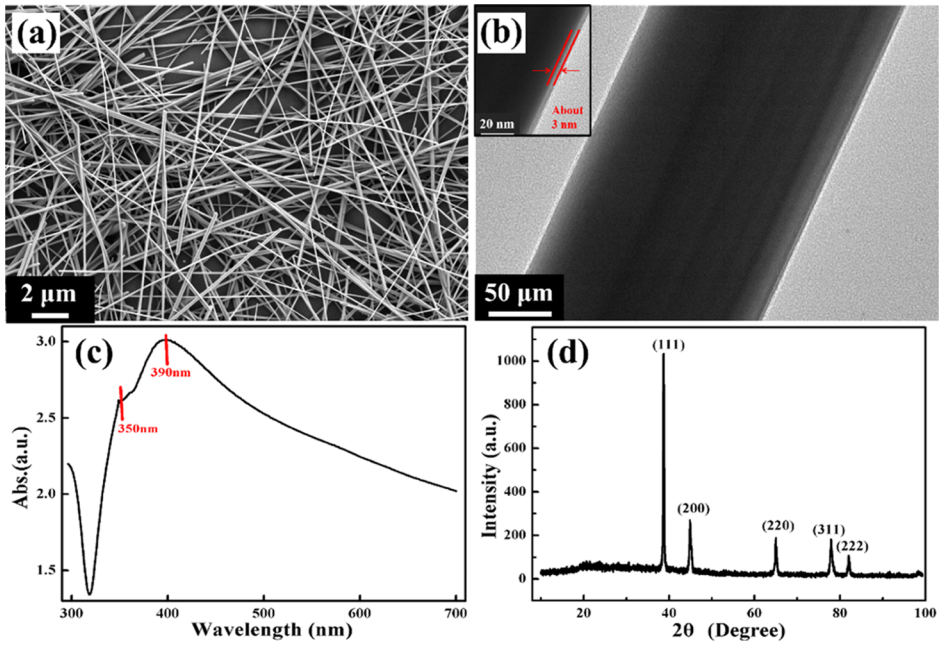

Figure 2. (a) SEM image, (b) TEM image, (c) UV−vis spectrum, and (d) XRD spectrum of the prepared AgNWs.

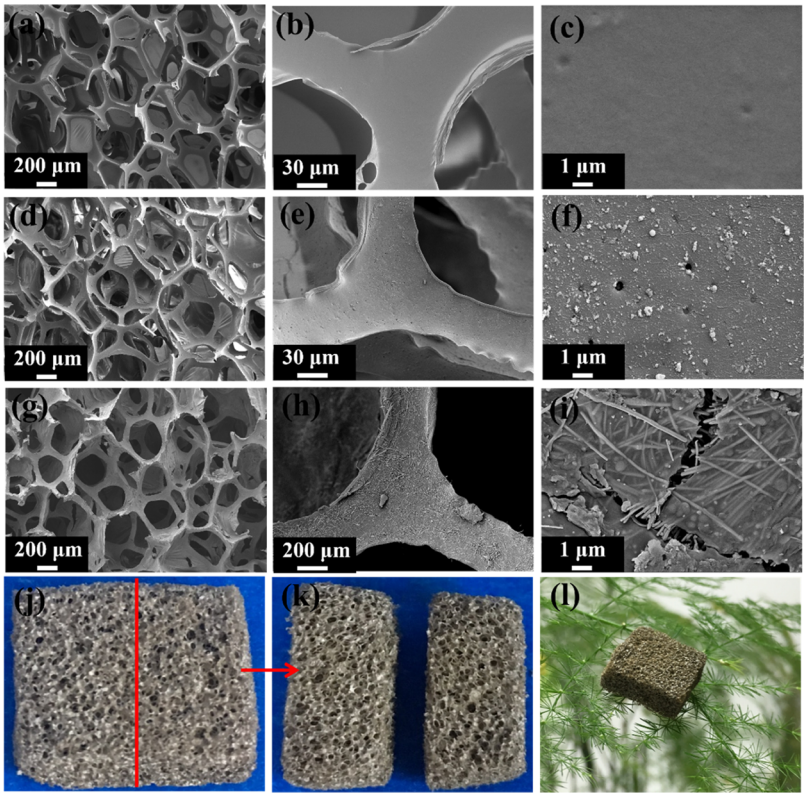

Figure 3. SEM images of (a−c) PU sponge, (d−f) PDA-treated PU sponge, and (g−i) CA@PU sponge at different magnifications; (j) uniform macrostructure and (k) fractured surfaces of the conductive CA@PU sponge; and (l) green leaf supports the conductive CA@PU sponge without being bent.

remove excess EG and PVP and redispersed in water, and the mass loading of the as-prepared AgNWs dispersion was fixed as 10 mg/mL for the following application.

2.3. Fabrication of Conductive CA@PU Sponge. As shown in Figure 1, the conductive CA@PU sponge was prepared using a simple dip-coating technique. Briefly, the commercial PU was first washed with acetone and then dipped into the DA/Tris buffer solution (PH ≈ 8.5) for 24 h at 30 °C to obtain the polydopamine (PDA)-modified PU sponge. The color of the PU sponge turned to be brown with the deposition of PDA. Next, the PDA-modified PU sponge was repeatedly dipped into the CA solution (2 mg/mL) with a mass ratio of 3:2 under ultrasonication for 10 min. Then, the excessive solution was squeezed out from the sponge followed by drying at 80 °C for 1 h, achieving a gray conductive CA@PU sponge. Here, the dipping number was labeled as *x*, and the corresponding sample was denoted as CA@PU$_x$.

DOI: 10.1021/acsami.9b00900
ACS Appl. Mater. Interfaces 2019, 11, 10922−10932

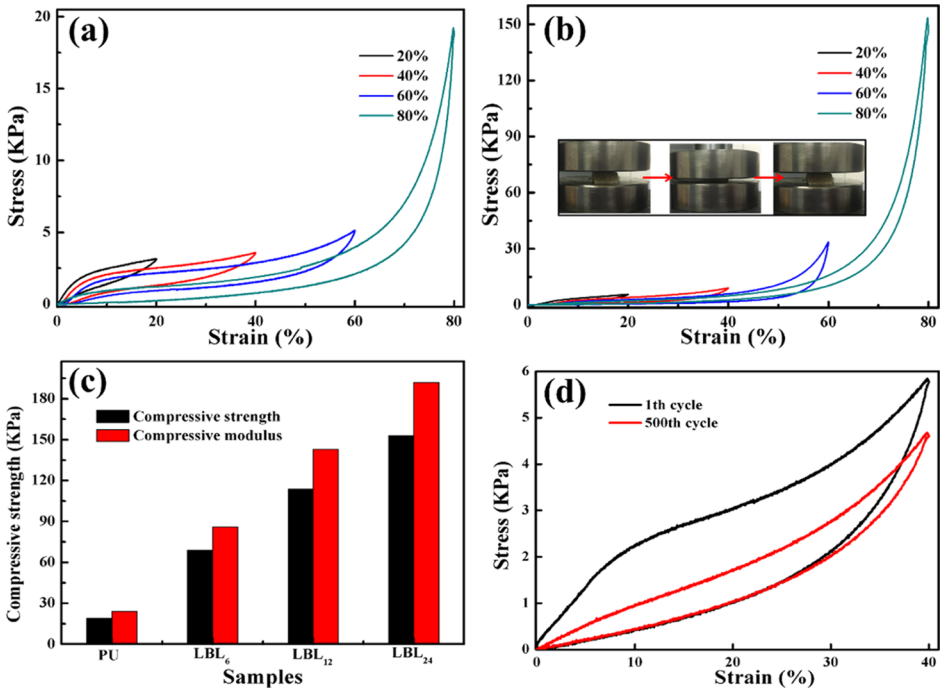

Figure 4. Compressive stress−strain curves of (a) PU sponge and (b) conductive CA@PU$_{24}$ sponge under different strains. The inset in (b) is the digital pictures, showing the ultrahigh compressibility and good recoverability of conductive CA@PU sponge; (c) compressive strength and compressive modulus of different CA@PU sponges; and (d) stress−strain curves of CA@PU$_{24}$ under 40% strain for the 1st and 500th cycles.

2.4. Preparation of Piezoresistive Sensor and Electronic Skin. In this study, the prepared conductive CA@PU sponge was applied with a precompression treatment to produce cracked structure on the surface of sponge skeleton, during which the sponge was first compressed to a strain of 80% at a rate of 5 mm/min and then returned to the initial state using a universal mechanical tester. For the piezoresistive sensor, conductive silver paste was applied to the two opposite faces of the cubic conductive CA@PU sponge (2 × 2 × 2 cm^3) to eliminate contact resistance and to collect stable resistance signal output. Then, conductive tapes were adhered to the two faces for resistance and piezoresistive sensing test. As for electronic skin, cubic conductive CA@PU sponges (1 × 1 × 1 cm^3) were used to construct 5 pixel × 5 pixel arrays on an insulating plastic plate. The surface and bottom of each sponge were coated with conductive silver paste, and then each row selection and each column selection were connected by a conductive tape.

2.5. Characterization. The micromorphology of sponge and AgNWs was observed through SEM (Zeiss MERLIN Compact) at an accelerating voltage of 5 kV. Transmission electron microscopy (TEM) was performed with a Tecnai G2 20 instrument at an acceleration voltage of 90 kV. X-ray diffraction (XRD) scans in the range of 10−100° were recorded using a Bruker-AXS D8 ADVANCE (Shimadzu Co. Ltd, XRD-6100) with Ni-filtered Cu Kα radiation (λ = 0.15418 nm) at a swing speed of 0.02°/min at 40 kV. The Fourier transform infrared spectroscopy (FTIR) spectrum in the range of 50−4000 cm^{-1} was collected on a Nicolet NEXUS 870 instrument at a resolution of 4 cm^{-1} using the attenuated total reflection mode. UV−vis absorption spectroscopy was performed on a UV−vis spectrophotometer (Agilent, Cary 5000) in the range from 300 to 700 nm. Cubic CA@PU sponges (2 × 2 × 2 cm^3) were subjected to a universal testing machine (Shimadzu, Japan) at a compression rate of 5 mm/min to investigate their compression performance. The I−V curves of the piezoresistive sensors were measured by an RST5000 electrochemical workstation (Suzhou Risetest Electronic Co., Ltd, China) with linear sweep voltammetry. The resistance of the piezoresistive sensor was tested using a digital multimeter (Tektronix DMM4050). Digital multimeter and universal tensile tester were used together to measure the piezoresistive sensing behavior of the sensor online.

3. RESULTS AND DISCUSSION

3.1. Characterizations of AgNWs. SEM and TEM were conducted to study the morphology of the prepared AgNWs. As shown in Figure 2a, AgNWs with an average length of 20−30 μm were obtained with very few silver nanoparticles, showing the high purity of AgNWs. The TEM image (see Figure 2b) displayed the diameter of AgNWs which is about 150 nm. Besides, about 3 nm thick PVP identified through FTIR (see Figure S1) was observed on the surface of AgNWs.[63] It is well known that the existence of PVP can effectively prevent the oxidation of AgNWs and improve the dispersity of AgNWs in water.[64] To further demonstrate the purity and the structure of AgNWs, UV−vis spectra (see Figure 2c) and XRD spectra (see Figure 2d) of AgNWs were characterized. Generally, the existence of the absorption peaks at 350/390 and 410 nm in the UV−vis spectrum is the characteristic peaks of long AgNWs and silver nanoparticles, respectively.[65,66] Hence, the absence of the absorption peak at 410 nm in Figure 2c also verified the high purity of the prepared AgNWs. As for the XRD spectrum of AgNWs, five characteristic diffraction peaks were observed at 2θ = 38.06, 44.26, 64.4, 77.34, and 81.48°, corresponding to the (111), (200), (220), (311), and (222) crystalline planes of pure face-centered cubic silver crystals, respectively.[6]

3.2. Characterizations of Conductive CA@PU Sponge. As shown in Figure 3a−c, the commercial PU sponge possessed an interconnected 3D porous structure with a pore diameter of 300−500 μm and smooth skeleton. After the self-polymerization of PDA, there was almost no obvious change about the interconnected 3D porous structure (see Figure 3d), but the surface of the sponge skeleton becomes rough because of the existence of wrinkled PDA layer (see Figure 3e). Here, PDA was applied to improve the hydrophilicity of PU sponge to facilitate the dip-coating process in the next step.[55] This can be verified from Figure S2 that the water contact angle (WCA)

DOI: 10.1021/acsami.9b00900
ACS Appl. Mater. Interfaces 2019, 11, 10922−10932

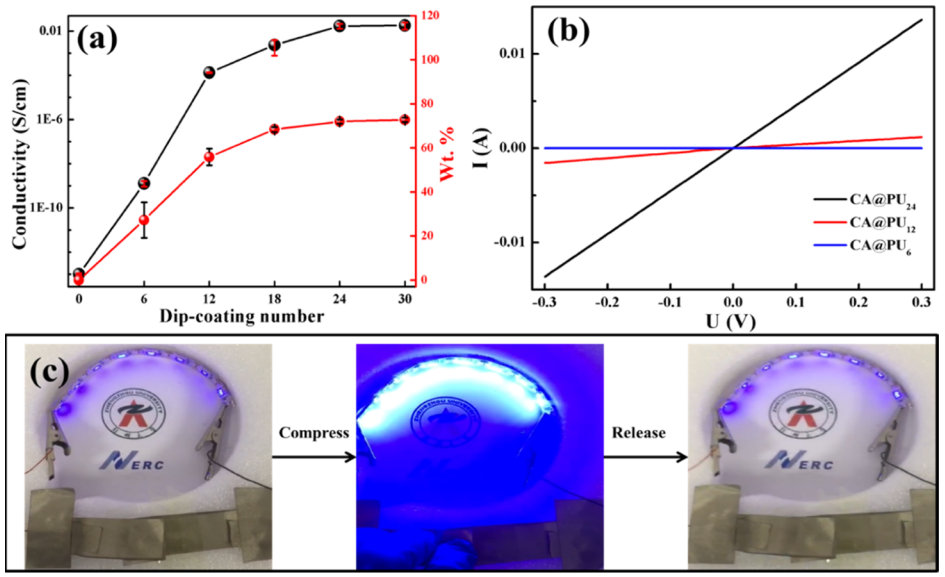

Figure 5. (a) Electrical conductivity and CA loading of conductive CA@PU sponge as a function of dip-coating number; (b) current−voltage characteristic curves of different CA@PU sponges; and (c) light intensity of the LED connected with the conductive CA@PU sponge changed with the compression and release of strain.

of the PU sponge decreased from 141° to 84°, indicating the transformation of PU sponge from hydrophobicity into hydrophilicity. Therefore, it can be clearly seen in Figure 3j that both the outer and fracture surfaces presented uniform gray in color, indicating that the CA solution can easily permeate into the porous structure. Meanwhile, the excellent adhesion of PDA can also enhance the adhesion strength between CA layer and PU skeleton.[67] After cyclic dip-coating in CA solution, the conductive CA@PU sponge also inherited the interconnected 3D porous structure of PU (see Figure 3g), but the roughness of the surface of the porous skeleton was further increased because of the homogeneous distribution of AgNWs (see Figure 3h). Besides, as expected, a cracked CA conductive layer was successfully constructed on the sponge skeleton (Figure 3i). Finally, a green leaf could support the conductive CA@PU sponge without being bent (see Figure 3k), indicating that the lightweight characteristic of PU sponge was well maintained.

3.3. Mechanical Property of Conductive CA@PU Sponge. Generally, good mechanical property is crucial for an ideal piezoresistive sensor. Here, a series of compression tests were conducted at a compression rate of 5 mm/min to study the mechanical property of PU sponge and different CA@PU sponges. As shown in Figure 4a, three typical distinct stages were observed for the compressive stress−strain curves of PU sponge:[68] the linear elastic region for $\varepsilon < 10\%$ within which the stress increased quickly and linearly; the plateau region for $10\% < \varepsilon < 60\%$ within which the stress increased slowly; and the densification region for $\varepsilon > 60\%$ within which the stress increased sharply. Besides, it can be clearly seen that the stress can almost completely return to the initial point for each strain when the PU sponge was unloaded, and very small residual strain was observed even for large strains of 60% and 80% (Figure S3). All of these indicated the excellent elasticity without plastic deformation of PU sponge. Next, the conductive CA@PU_{24} sponge was also subjected to different strains to investigate the influence of the CA layer coating on the mechanical property of PU sponge. The sponge could almost fully recover to its initial shape even after being compressed to 80% strain (insect of Figure 4b). Besides, compared with PU sponge, the compressive stress−strain curves of conductive CA@PU_{24} also displayed three distinct regions (see Figure 4b). However, small residual strains of 2 and 5.6% were observed after unloading from 60 to 80% strains, respectively. This indicated that the introduction of conductive CA layer would reduce the elasticity of the PU sponge upon higher external compressive strain. Meanwhile, it can also be concluded from the compressive stress−strain curves of different CA@PU sponges in Figures S4 and 4C that both the compressive strength and the compressive modulus increased with increasing dip-coating number. All of these are ascribed to the high modulus of cellulose[60] and the rigidity of AgNWs.[61] Finally, the conductive CA@PU sponge was subjected to cyclic compression test under 40% strain at a compression rate of 5 mm/min, and the typical compressive stress−strain curves for the first and 500th cycles are displayed in Figure 4d. Compared with the hysteresis loop of the first cycle, a shrinkage of the hysteresis loop was observed for the 500th cycle and the maximum stress decreased from 5.8 to 4.6 kPa at the 40% strain. It indicated the excellent mechanical fatigue resisting performance of the CA@PU sponge. Meanwhile, there was still no residual strain after 500 cycles, showing excellent compressibility and recoverability. All of these are very important for the durability and reproductivity of ideal piezoresistive sensor.

3.4. Electrical Property of Conductive CA@PU Sponge. As shown in Figure 5a, the electrical conductivity and the CA loading of conductive CA@PU sponge as a function of dip-coating number were investigated. Observably, the conductivity increased sharply from 1×10^{-13} to 1.3×10^{-4} S/cm after coating 12 times, indicating that the conductive networks had been constructed. With further increase of coating number, the conductivity increased slightly and tended to be stable since the 24th cycle, which demonstrated that the conductive network had reached the stable state. The dip-coating number-dependent phenomenon is mainly related to the conductive CA layer loading which exhibited the similar trend. That is to say, more effective

DOI: 10.1021/acsami.9b00900
ACS Appl. Mater. Interfaces 2019, 11, 10922−10932

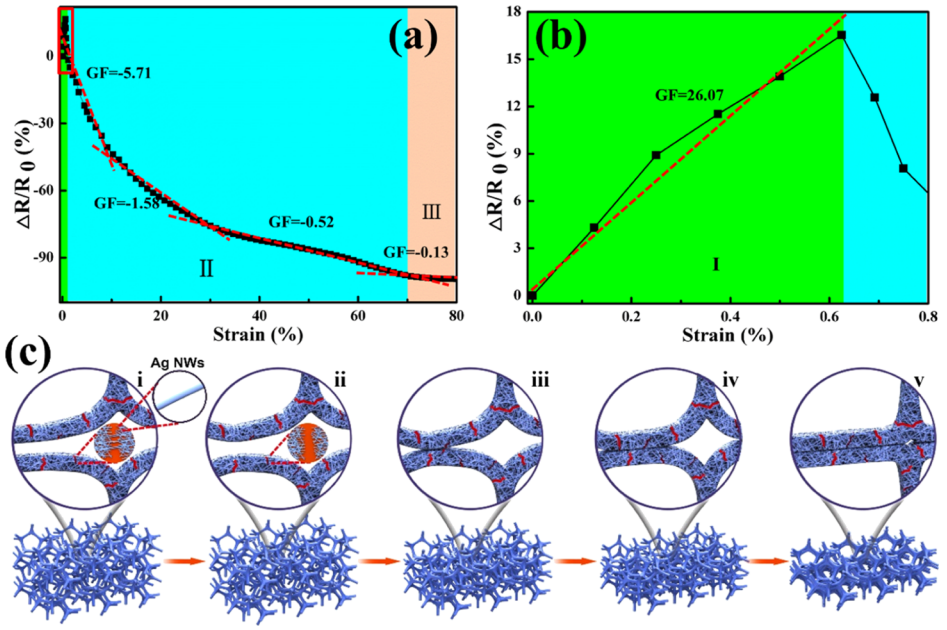

Figure 6. (a) $\Delta R/R_0$ of conductive CA@PU_{24} sponge with increasing compression strain; (b) enlarged picture of the rectangle part in (a); and (c) schematic evolutions of the porous structure with increasing compression strain.

conductive networks were established with increasing CA loading. Hence, the electrical property of the CA@PU sponge could be effectively tuned through changing the coating number. In addition, the $I-V$ curves of different conductive CA@PU sponges were tested and are displayed in Figure 5b. All of the samples exhibited good linear ohmic behaviors, indicating good stability of the electrical property.[69] This is very important for the sensor to perform stable sensing behavior. Finally, the conductive CA@PU sponge was connected with a blue light-emitting diode (LED) to visualize the piezoresistive effect of the sponge. It can be clearly observed that the brightness of the LED became stronger upon external compression strain and dimmed after releasing strain (see Figure 5c and Video S1). All of these indicated the great potential of as-prepared CA@PU sponge to serve as a piezoresistive sensor.

3.5. Piezoresistive Property of Conductive CA@PU Sponge. Figure 6a,b displays the typical relationship between resistance variation ratio ($\Delta R/R_0 = (R - R_0)/R_0$, where R and R_0 correspond to the resistance with and without compression strain,[70] respectively) and compression strain (up to 80%) of CA@PU_{24} at a compression rate of 5 mm/min. The corresponding schematic evolutions of the porous structure are also illustrated in Figure 6c. Obviously, the whole sensing range can be divided into three distinct regions, which are closely associated with the variation of the porous structure. In region I ($0 < \varepsilon < 0.6\%$, Figure 6b), it can be clearly seen that the resistance increased sharply in such a small-strain range, which is attributed to the cracked CA layer located on the sponge skeleton, as shown in Figure 6c-i. Based on the "crack effect" illustrated in Figure 6c-ii, the bending of the porous skeleton upon external compression would lead to the open and expansion of the crack, resulting in the breakage of local conductive pathways and sharp resistance increase of the conductive CA@PU sponge. With the further increase of applied strain ($0.6 < \varepsilon < 70\%$, region II), the resistance decreased rapidly at first and then slowly. This is due to the "contact effect" between adjacent sponge skeletons which suppressed the "crack effect" under higher strain, leading to the construction of perfect conductive pathways and the decrease of resistance. Here, two different contact modes are applied to explain the changing resistance variation ratio. Initially, the "point contact" in Figure 6c-iii is the main contact mode, causing the sharp increase of the number of conductive paths. After that, the "point contact" gradually evolved into "area contact" with increasing compression strain (Figure 6c-iv). Generally, "area contact" meant that the conductive network has reached a stable state; there will be no obvious variation of resistance upon further compression. Hence, the decrease rate of resistance reduced gradually. For region III ($70\% < \varepsilon < 80\%$), "area contact" turned to be the main contact mode because of the densification of porous sponge at high strain (Figure 6c-iv). Here, almost all of the porous skeleton of sponge contacted with each other, and the tunnel distance between the conductive CA layer decreased upon external compression, causing the reduction of tunneling resistance. Hence, the resistance exhibited a relative small variation compared with that in regions I and II. Additionally, the gauge factor (GF, $GF = (\Delta R/R_0)/\varepsilon$, where ΔR, R_0, and ε represents the instantaneous resistance change, original resistance, and strain applied, respectively) was also applied to evaluate the sensitivity of the piezoresistive sensor. In region I, the GF was calculated to be about 26.07, which is much higher than that of the CB@PU sponge (GF = 2.2),[39] gold@PU (GF = 1.09),[52] and MWCNT/RGO/PU (GF = 1.52)[30] in small strain range of 0−0.6%. Therefore, the conductive CA@PU served as a piezoresistive sensor possesses ultrahigh sensitivity toward small strain. For region II, the GF first decreased from −5.71 to −1.58 and then to −0.52 with increasing compression strain. In the last region III, the GF became to be only −0.13, indicating that the further compression has relative weak effect on the conductive networks. Overall, the "crack effect" and "contact effect" worked together to endow the piezoresistive sensor with low detect limit and wide detect range.[52]

Next, cyclic piezoresistive behaviors of the sensor to different compression strains were systematically studied. For

DOI: 10.1021/acsami.9b00900
ACS Appl. Mater. Interfaces 2019, 11, 10922−10932

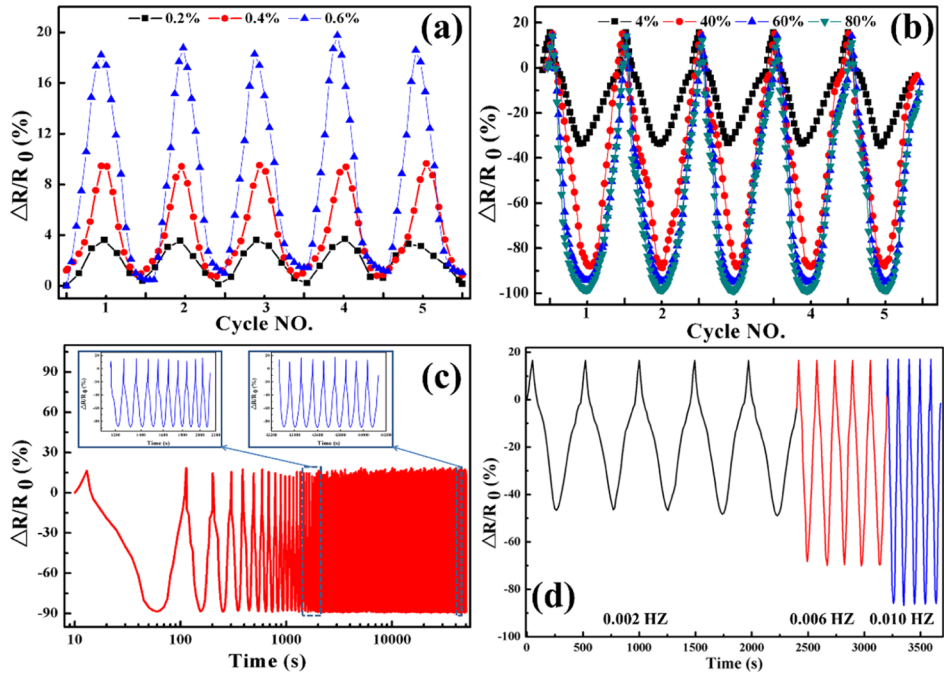

Figure 7. Cyclic piezoresistive behavior of conductive CA@PU_{24} sponge under (a) small (0.2, 0.4, and 0.6%) and (b) large (4, 40, 60, and 80%) compression strains; (c) stability test of the piezoresistive behavior of conductive CA@PU_{24} sponge under a compression strain of 40% at a compression rate of 5 mm/min for 500 cycles; and (d) frequency dependence of the piezoresistive behavior of conductive CA@PU_{24} sponge.

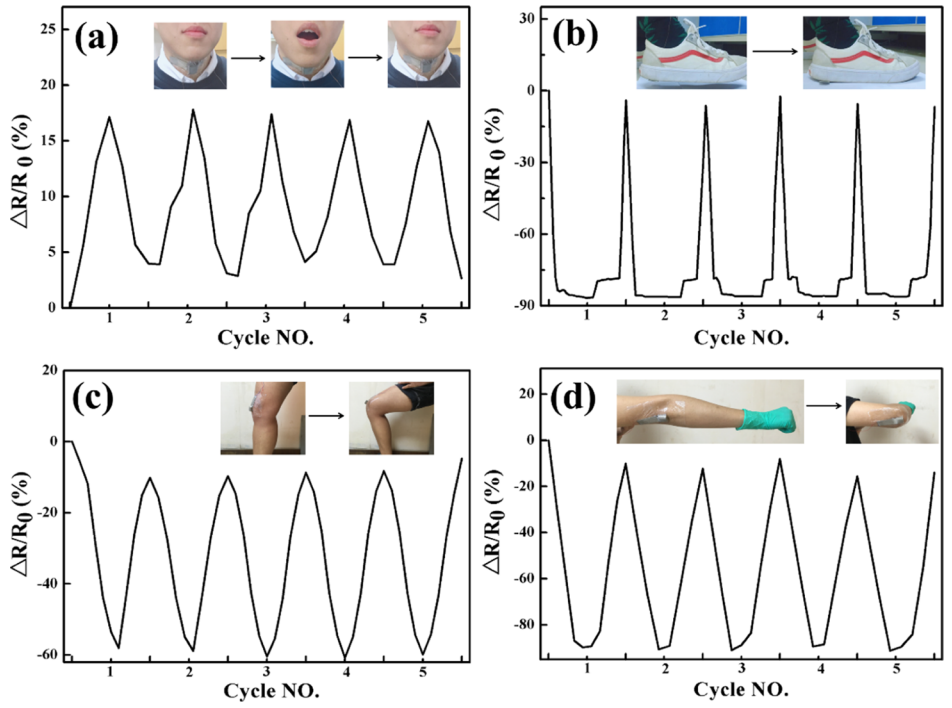

Figure 8. Resistance variation signals of the conductive CA@PU sponge when detecting the human bodily motions, including (a) phonation, (b) stamping, (c) knee bending, and (d) wrist bending.

each compression cycle, based on the "crack effect" in the small-strain range, the resistance was increased linearly by about 3.6, 9.24, and 18.7% toward 0.2, 0.4, and 0.6% strain, respectively (Figure 7a). Meanwhile, the resistance was decreased by about 33.7, 87.9, 95.1, and 98.6% toward 4, 40, 60, and 80% strain because of the "contact effect" (Figure 7b) in the large strain range, respectively. After releasing the strain, because of the excellent compression-resilience properties of the sponge, the resistance almost fully recovered to its initial value for both small and large strain ranges, showing excellent recoverability. Importantly, the sensor also displayed stable repeatability under different compression strains, which is very crucial for its practical applications. Notably, a compressive strain as low as 0.2% could be effectively detected, endowing the sensor with the capability of discerning small motion, such as pulse, heart monitoring, and speech. To detect the durability

DOI: 10.1021/acsami.9b00900
ACS Appl. Mater. Interfaces 2019, 11, 10922−10932

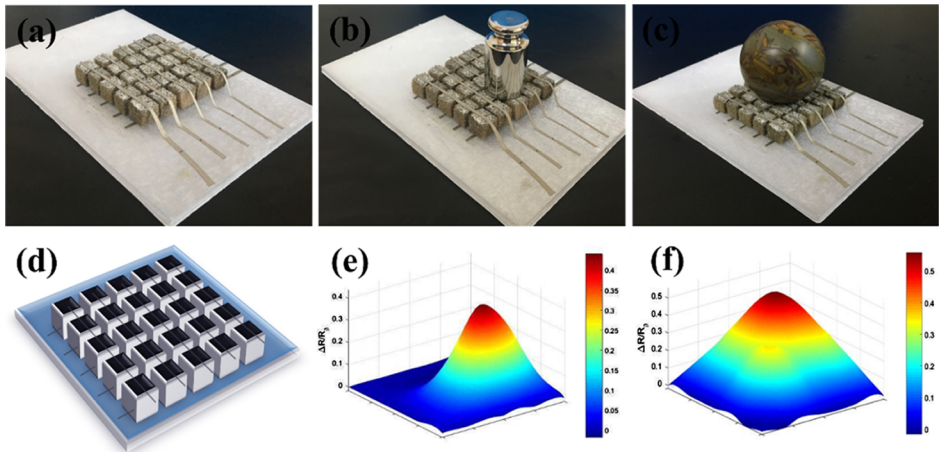

Figure 9. (a) Digital photo of a CA@PU-based artificial electronic skin with 5 × 5 pixels; photographs of (b) 100 g weight and (c) stone ball located onto the surface of as-prepared artificial electronic skin; (d) schematic diagram of the artificial electronic skin with 5 × 5 pixels; and (e,f) corresponding maps of estimated pressure profile over a 3D area based on the change in resistance.

of the sensor, the piezoresistive behavior under 40% strain during 500 cycles was conducted. As displayed in Figure 7c, the response pattern kept almost unchanged in each cycle. The resistance of the sensor increased first due to the open of cracks and then decreased arising from the contact of the skeleton of PU sponge upon external compression. After releasing the compression strain, the resistance completely restored to its initial value based on the recovery of the conductive network. All these are ascribed to the stable compression mechanical property of the sponge. Finally, the frequency dependence of the piezoresistive behavior of the sponge was evaluated, and an increase trend in sensitivity with increasing frequency was observed (Figure 7d). The frequency-dependent piezoresistive behavior will undoubtly enhance the discernibility of the piezoresistive sensor.

3.6. Applications in Human Motion Detection. As discussed above, the piezoresistive sensor possesses high sensitivity toward small and large strains. To disclose its feasibility in the wearable electronic device, a series of tests were conducted to detect different human motions. First, the sensor was adhered to the throat using a medical waterproof tape to detect the small motion caused by phonation (Figure 8a). As a result, significant resistance variation was accurately recorded because of the small compression and release induced by the throat when the tester made a sound. Besides, the sensor also exhibited excellent stability and repeatability upon repeated pronunciation. Hence, the sponge sensor possessed great potential to act as a voice recognition device. As for the large-scale motions, the sensor was fixed to the sole of the shoe to detect the stamping. As expected, the sensor displayed sharp and repeatable resistance variation signal upon consecutive stamping (Figure 8b), which impose great compression to the sensor. Meanwhile, the sensor was attached onto the knee and wrist to detect their movements. Obviously, the sponge also demonstrated outstanding stable and reproducible response patters upon the bending of knee and wrist (Figure 8c,d). All of these indicated that the piezoresistive sensor possesses great potential in the fields of human health and sports monitoring.

3.7. Electronic Skin. Based on the excellent compressibility and piezoresistive performance of the conductive CA@PU sponge, cubic samples were integrated into 5 × 5 pixels to investigate its potential applications in a compression-sensitive artificial electronic skin (Figure 9a). The schematic diagram of the artificial electronic skin is illustrated in Figure 9d. The color contrast mapped with external applied pressure according to the resistance variation ratio of each pixel was plotted. As shown in Figure 9b, a 100 g weight was placed onto the surface of the artificial electronic skin; it can be obviously observed the significant difference of resistance variation ratio based on the different applied pressures at different locations. Meanwhile, the corresponding resistance variation ratio in Figure 9e is consistent with the location and shape of the weight. Similarly, as shown in Figure 9c, a stone ball located on the surface of artificial electronic skin could also be accurately monitored through the color contrast map in Figure 9f. The results demonstrated the great potential of the CA@PU sponge-based artificial electronic skin to detect the location and shape of the external object. To fulfill the scale production of the CA@PU sponge-based artificial electronic skin in the future, the precise control of the precompression process that produce the ultrasensitive crack structure is very crucial. In addition, advanced technique such as the photolithography technique could be applied to fabricate electronic skins with more pixels, which will be helpful for the improvement of the resolution of CA@PU electronic skin.

4. CONCLUSIONS

In summary, a conductive CA@PU sponge was successfully prepared through repeatedly dipping the PU sponge into CNF/AgNW solution. It is noted that the mechanical and electrical properties of the conductive CA@PU sponge could be adjusted by changing the dip-coating number. With the increase of dip-coating number, both of the compressive strength and compressive modulus of the sponge increased due to the high modulus of cellulose and the rigidity of AgNWs. Meanwhile, the electrical conductivity was also enhanced based on the progressive construction of effective conductive networks. As a piezoresistive sensor, a cracked structure was effectively constructed in the conductive CA layer through a precompression strain up to 80% at a rate of 5 mm/min. Hence, the conductive CA@PU sponge exhibited a detection limit as low as 0.2% and an ultrahigh GF of 26.07 based on the "crack effect" for small strain. In addition, it also displayed exceptional stability, repeatability, and durability for a larger compression strain up to 80% because of the "contact effect". All of these excellent sensing characteristics made it applicable

DOI: 10.1021/acsami.9b00900
ACS Appl. Mater. Interfaces 2019, 11, 10922−10932

for the detection of various human bodily motions, such as phonation, stamping, knee bending, and wrist bending. Most importantly, the sponge also exhibited great potential for the fabrication of artificial electronic skin. We believe that this simple design will undoubtedly promote the development of high-performance flexible wearable electronics.

■ ASSOCIATED CONTENT

Supporting Information

The Supporting Information is available free of charge on the ACS Publications website at DOI: 10.1021/acsami.9b00900.

FTIR spectrums of as-prepared AgNWs and PVP; WCA of original PU sponge and PDA-treated PU sponge; residual strain of the PU sponge after 60 and 80% compression strains; and compressive stress−strain curves of CA@PU_6 sponge and CA@PU_{12} sponge under different strains (PDF)

Light intensity of the LED connected with the conductive CA@PU sponge changed with the compression and release of strain (AVI)

■ AUTHOR INFORMATION

Corresponding Author

*E-mail: liuhu@zzu.edu.cn (H.L.).

ORCID

Hu Liu: 0000-0003-3840-8135

Liwei Mi: 0000-0001-9239-6599

Chuntai Liu: 0000-0001-9751-6270

Zhanhu Guo: 0000-0003-0134-0210

Notes

The authors declare no competing financial interest.

■ ACKNOWLEDGMENTS

The authors gratefully acknowledge the financial support of this work by National Natural Science Foundation of China (contract numbers: 51803191, 11572290, and 11432003), China Postdoctoral Science Foundation (2018M642782), the 111 project (D18023), and the National Key Research and Development Program of China (2016YFB0101602). H.L. appreciates the start-up fund from Zhengzhou University.

■ REFERENCES

(1) Farcau, C.; Moreira, H.; Viallet, B.; Grisolia, J.; Ciuculescu-Pradines, D.; Amiens, C.; Ressier, L. Monolayered Wires of Gold Colloidal Nanoparticles for High-Sensitivity Strain Sensing. *J. Phys. Chem. C* **2011**, *115*, 14494−14499.

(2) Zheng, M.; Li, W.; Xu, M.; Xu, N.; Chen, P.; Han, M.; Xie, B. Strain Sensors Based on Chromium Nanoparticle Arrays. *Nanoscale* **2014**, *6*, 3930−3933.

(3) Hua, Q.; Sun, J.; Liu, H.; Bao, R.; Yu, R.; Zhai, J.; Pan, C.; Wang, Z. L. Skin-Inspired Highly Stretchable and Conformable Matrix Networks for Multifunctional Sensing. *Nat. Commun.* **2018**, *9*, 244.

(4) Wang, C.; Hwang, D.; Yu, Z.; Takei, K.; Park, J.; Chen, T.; Ma, B.; Javey, A. User-Interactive Electronic Skin for Instantaneous Pressure Visualization. *Nat. Mater.* **2013**, *12*, 899−904.

(5) Chortos, A.; Liu, J.; Bao, Z. Pursuing Prosthetic Electronic Skin. *Nat. Mater.* **2016**, *15*, 937−950.

(6) Lu, L.; Wei, X.; Zhang, Y.; Zheng, G.; Dai, K.; Liu, C.; Shen, C. A Flexible and Self-Formed Sandwich Structure Strain Sensor Based on AgNW Decorated Electrospun Fibrous Mats with Excellent Sensing Capability and Good Oxidation Inhibition Properties. *J. Mater. Chem. C* **2017**, *5*, 7035−7042.

(7) Liu, H.; Li, Q.; Zhang, S.; Yin, R.; Liu, X.; He, Y.; Dai, K.; Shan, C.; Guo, J.; Liu, C.; Shen, C.; Wang, X.; Wang, N.; Wang, Z.; Wei, R.; Guo, Z. Electrically Conductive Polymer Composites for Smart Flexible Strain Sensors: A Critical Review. *J. Mater. Chem. C* **2018**, *6*, 12121−12141.

(8) Wang, X.; Sun, H.; Yue, X.; Yu, Y.; Zheng, G.; Dai, K.; Liu, C.; Shen, C. A Highly Stretchable Carbon Nanotubes/Thermoplastic Polyurethane Fiber-Shaped Strain Sensor with Porous Structure for Human Motion Monitoring. *Compos. Sci. Technol.* **2018**, *168*, 126−132.

(9) Pang, C.; Lee, G.-Y.; Kim, T.-i.; Kim, S. M.; Kim, H. N.; Ahn, S.-H.; Suh, K.-Y. A flexible and highly sensitive strain-gauge sensor using reversible interlocking of nanofibres. *Nat. Mater.* **2012**, *11*, 795−801.

(10) Yang, Y.; Gao, W. Wearable and Flexible Electronics for Continuous Molecular Monitoring. *Chem. Soc. Rev.* **2018**, DOI: 10.1039/c7cs00730b.

(11) Liao, X.; Song, W.; Zhang, X.; Huang, H.; Wang, Y.; Zheng, Y. Directly printed wearable electronic sensing textiles towards human-machine interfaces. *J. Mater. Chem. C* **2018**, *6*, 12841−12848.

(12) Li, J.; Bao, R.; Tao, J.; Peng, Y.; Pan, C. Recent Progress in Flexible Pressure Sensor Arrays: From Design to Applications. *J. Mater. Chem. C* **2018**, *6*, 11878−11892.

(13) Huang, S.; He, G.; Yang, C.; Wu, J.; Guo, C.; Hang, T.; Li, B.; Yang, C.; Liu, D.; Chen, H.-J.; Wu, Q.; Gui, X.; Deng, S.; Zhang, Y.; Liu, F.; Xie, X. Stretchable Strain Vector Sensor Based on Parallelly Aligned Vertical Graphene. *ACS Appl. Mater. Interfaces* **2019**, *11*, 1294−1302.

(14) Gao, J.; Wang, X.; Zhai, W.; Liu, H.; Zheng, G.; Dai, K.; Mi, L.; Liu, C.; Shen, C. Ultrastretchable Multilayered Fiber with A Hollow-Monolith Structure for High-Performance Strain Sensor. *ACS Appl. Mater. Interfaces* **2018**, *10*, 34592−34603.

(15) Ren, M.; Zhou, Y.; Wang, Y.; Zheng, G.; Dai, K.; Liu, C.; Shen, C. Highly Stretchable and Durable Strain Sensor Based on Carbon Nanotubes Decorated Thermoplastic Polyurethane Fibrous Network with Aligned Wave-Like Structure. *Chem. Eng. J.* **2019**, *360*, 762−777.

(16) Wang, Y.; Jia, Y.; Zhou, Y.; Wang, Y.; Zheng, G.; Dai, K.; Liu, C.; Shen, C. Ultra-Stretchable, Sensitive and Durable Strain Sensors Based on Polydopamine Encapsulated Carbon Nanotubes/Elastic bands. *J. Mater. Chem. C* **2018**, *6*, 8160−8170.

(17) Liu, H.; Zhu, L.-l.; He, Y.; Cheng, B.-w. A Novel Method for Fabricating Elastic Conductive Polyurethane Filaments by In-Situ Reduction of Polydopamine and Electroless Silver Plating. *Mater. Des.* **2017**, *113*, 254−263.

(18) Zheng, Y.; Li, Y.; Li, Z.; Wang, Y.; Dai, K.; Zheng, G.; Liu, C.; Shen, C. The Effect of Filler Dimensionality on The Electromechanical Performance of Polydimethylsiloxane Based Conductive Nanocomposites for Flexible Strain Sensors. *Compos. Sci. Technol.* **2017**, *139*, 64−73.

(19) Zhang, L.; Li, H.; Lai, X.; Gao, T.; Yang, J.; Zeng, X. Thiolated Graphene@Polyester Fabric-Based Multilayer Piezoresistive Pressure Sensors for Detecting Human Motion. *ACS Appl. Mater. Interfaces* **2018**, *10*, 41784−41792.

(20) Wu, X.; Han, Y.; Zhang, X.; Lu, C. Highly Sensitive, Stretchable, and Wash-Durable Strain Sensor Based on Ultrathin Conductive Layer@Polyurethane Yarn for Tiny Motion Monitoring. *ACS Appl. Mater. Interfaces* **2016**, *8*, 9936−9945.

(21) Chen, S.; Wei, Y.; Yuan, X.; Lin, Y.; Liu, L. A highly Stretchable Strain Sensor Based on A Graphene/Silver Nanoparticle Synergic Conductive Network and A Sandwich Structure. *J. Mater. Chem. C* **2016**, *4*, 4304−4311.

(22) Chen, S.; Wei, Y.; Wei, S.; Lin, Y.; Liu, L. Ultrasensitive Cracking-Assisted Strain Sensors Based on Silver Nanowires/Graphene Hybrid Particles. *ACS Appl. Mater. Interfaces* **2016**, *8*, 25563−25570.

(23) Wu, J.; Wang, H.; Su, Z.; Zhang, M.; Hu, X.; Wang, Y.; Wang, Z.; Zhong, B.; Zhou, W.; Liu, J.; Xing, S. G. Highly Flexible and Sensitive Wearable E-Skin Based on Graphite Nanoplatelet and Polyurethane Nanocomposite Films in Mass Industry Production Available. *ACS Appl. Mater. Interfaces* **2017**, *9*, 38745−38754.

(24) Gong, T.; Zhang, H.; Huang, W.; Mao, L.; Ke, Y.; Gao, M.; Yu, B. Highly Responsive Flexible Strain Sensor Using Polystyrene Nanoparticle Doped Reduced Graphene Oxide for Human Health Monitoring. *Carbon* **2018**, *140*, 286−295.
(25) Zhang, Y.; Fang, Y.; Li, J.; Zhou, Q.; Xiao, Y.; Zhang, K.; Luo, B.; Zhou, J.; Hu, B. Dual-Mode Electronic Skin with Integrated Tactile Sensing and Visualized Injury Warning. *ACS Appl. Mater. Interfaces* **2017**, *9*, 37493−37500.
(26) Ma, L.; Shuai, X.; Hu, Y.; Liang, X.; Zhu, P.; Sun, R.; Wong, C.-p. A Highly Sensitive and Flexible Capacitive Pressure Sensor Based on A Micro-Arrayed Polydimethylsiloxane Dielectric Layer. *J. Mater. Chem. C* **2018**, *6*, 13232−13240.
(27) Jeong, J.-H.; Xu, J.; Jo, H.; Li, J.; Kong, X.; Collins, W.; Bennett, C.; Laflamme, S. Development of Wireless Sensor Node Hardware for Large-Area Capacitive Strain Monitoring. *Smart Mater. Struct.* **2019**, *28*, 015002.
(28) You, X.; He, J.; Nan, N.; Sun, X.; Qi, K.; Zhou, Y.; Shao, W.; Liu, F.; Cui, S. Stretchable Capacitive Fabric Electronic Skin Woven by Electrospun Nanofiber Coated Yarns for Detecting Tactile and Multimodal Mechanical Stimuli. *J. Mater. Chem. C* **2018**, *6*, 12981−12991.
(29) Wei, X.; Cao, X.; Wang, Y.; Zheng, G.; Dai, K.; Liu, C.; Shen, C. Conductive Herringbone Structure Carbon Nanotube/Thermoplastic Polyurethane Porous Foam Tuned by Epoxy for High Performance Flexible Piezoresistive Sensor. *Compos. Sci. Technol.* **2017**, *149*, 166−177.
(30) Ma, Z.; Wei, A.; Ma, J.; Shao, L.; Jiang, H.; Dong, D.; Ji, Z.; Wang, Q.; Kang, S. Lightweight, Compressible and Electrically Conductive Polyurethane Sponges Coated with Synergistic Multi-walled Carbon Nanotubes and Graphene for Piezoresistive Sensors. *Nanoscale* **2018**, *10*, 7116−7126.
(31) Huang, W.; Dai, K.; Zhai, Y.; Liu, H.; Zhan, P.; Gao, J.; Zheng, G.; Liu, C.; Shen, C. Flexible and Lightweight Pressure Sensor Based on Carbon Nanotube/Thermoplastic Polyurethane-Aligned Conductive Foam with Superior Compressibility and Stability. *ACS Appl. Mater. Interfaces* **2017**, *9*, 42266−42277.
(32) Kuang, J.; Liu, L.; Gao, Y.; Zhou, D.; Chen, Z.; Han, B.; Zhang, Z. A Hierarchically Structured Graphene Foam and Its Potential as A Large-Scale Strain-Gauge Sensor. *Nanoscale* **2013**, *5*, 12171−12177.
(33) Ku-Herrera, J. J.; Avilés, F. Cyclic Tension and Compression Piezoresistivity of Carbon Nanotube/Vinyl Ester Composites in The Elastic and Plastic Regimes. *Carbon* **2012**, *50*, 2592−2598.
(34) Wang, M.; Zhang, K.; Dai, X.-X.; Li, Y.; Guo, J.; Liu, H.; Li, G.-H.; Tan, Y.-J.; Zeng, J.-B.; Guo, Z. Enhanced Electrical Conductivity and Piezoresistive Sensing in Multi-Wall Carbon Nanotubes/Polydimethylsiloxane Nanocomposites via The Construction of A Self-Segregated Structure. *Nanoscale* **2017**, *9*, 11017−11026.
(35) Bai, P.; Zhu, G.; Jing, Q.; Yang, J.; Chen, J.; Su, Y.; Ma, J.; Zhang, G.; Wang, Z. L. Membrane-Based Self-Powered Triboelectric Sensors for Pressure Change Detection and Its Uses in Security Surveillance and Healthcare Monitoring. *Adv. Funct. Mater.* **2014**, *24*, 5807−5813.
(36) Wang, N.; Xu, Z.; Zhan, P.; Dai, K.; Zheng, G.; Liu, C.; Shen, C. A tunable Strain Sensor Based on A Carbon Nanotubes/Electrospun Polyamide 6 Conductive Nanofibrous Network Embedded into Poly(vinyl alcohol) with Self-Diagnosis Capabilities. *J. Mater. Chem. C* **2017**, *5*, 4408−4418.
(37) Liu, H.; Li, Y.; Dai, K.; Zheng, G.; Liu, C.; Shen, C.; Yan, X.; Guo, J.; Guo, Z. Electrically Conductive Thermoplastic Elastomer Nanocomposites at Ultralow Graphene Loading Levels for Strain Sensor Applications. *J. Mater. Chem. C* **2016**, *4*, 157−166.
(38) (a) Yan, C.; Wang, J.; Kang, W.; Cui, M.; Wang, X.; Foo, C. Y.; Chee, K. J.; Lee, P. S. Highly Stretchable Piezoresistive Graphene-Nanocellulose Nanopaper for Strain Sensors. *Adv. Mater.* **2014**, *26*, 2022−2027. (b) Gong, T.; Liu, M.-Q.; Liu, H.; Peng, S.-P.; Li, T.; Bao, R.-Y.; Yang, W.; Xie, B.-H.; Yang, M.-B.; Guo, Z. Selective Distribution and Migration of Carbon Nanotubes Enhanced Electrical and Mechanical Performances in Polyolefin Elastomers. *Polymer* **2017**, *110*, 1−11.
(39) Wu, X.; Han, Y.; Zhang, X.; Zhou, Z.; Lu, C. Large-Area Compliant, Low-Cost, and Versatile Pressure-Sensing Platform Based on Microcrack-Designed Carbon Black@Polyurethane Sponge for Human-Machine Interfacing. *Adv. Funct. Mater.* **2016**, *26*, 6246−6256.
(40) Li, Y.; Liu, H.; Dai, K.; Zheng, G.; Liu, C.; Chen, J.; Shen, C. Tuning of Vapor Sensing Behaviors of Eco-Friendly Conductive Polymer Composites Utilizing Ramie Fiber. *Sens. Actuators, B* **2015**, *221*, 1279−1289.
(41) Wang, C.; Xia, K.; Wang, H.; Liang, X.; Yin, Z.; Zhang, Y. Advanced Carbon for Flexible and Wearable Electronics. *Adv. Mater.* **2018**, *31*, 1801072.
(42) (a) Hodlur, R. M.; Rabinal, M. K. Self Assembled Graphene Layers on Polyurethane Foam as A Highly Pressure Sensitive Conducting Composite. *Compos. Sci. Technol.* **2014**, *90*, 160−165. (b) Zhou, H.; Deng, H.; Zhang, L.; Fu, Q. Significant Enhancement of Thermal Conductivity in Polymer Composite via Constructing Macroscopic Segregated Filler Networks. *ACS Appl. Mater. Interfaces* **2017**, *9*, 29071−29081.
(43) Hu, H.; Zhao, Z.; Wan, W.; Gogotsi, Y.; Qiu, J. Polymer/Graphene Hybrid Aerogel with High Compressibility, Conductivity, and "Sticky" Superhydrophobicity. *ACS Appl. Mater. Interfaces* **2014**, *6*, 3242−3249.
(44) Tung, T. T.; Robert, C.; Castro, M.; Feller, J. F.; Kim, T. Y.; Suh, K. S. Enhancing The Sensitivity of Graphene/Polyurethane Nanocomposite Flexible Piezo-Resistive Pressure Sensors with Magnetite Nano-Spacers. *Carbon* **2016**, *108*, 450−460.
(45) Chen, L.; Chen, G. H.; Lu, L. Piezoresistive Behavior Study on Finger-Sensing Silicone Rubber/Graphite Nanosheet Nanocomposites. *Adv. Funct. Mater.* **2007**, *17*, 898−904.
(46) (a) Wang, M.; Shao, C.; Zhou, S.; Yang, J.; Xu, F. Super-compressible, fatigue resistant and anisotropic carbon aerogels for piezoresistive sensors. *Cellulose* **2018**, *25*, 7329−7340. (b) Zhou, X.; Zhu, L.; Fan, L.; Deng, H.; Fu, Q. Fabrication of Highly Stretchable, Washable, Wearable, Water-Repellent Strain Sensors with Multi-Stimuli Sensing Ability. *ACS Appl. Mater. Interfaces* **2018**, *10*, 31655−31663.
(47) Yu, S.; Wang, X.; Xiang, H.; Zhu, L.; Tebyetekerwa, M.; Zhu, M. Superior Piezoresistive Strain Sensing Behaviors of Carbon Nanotubes in One-Dimensional Polymer Fiber Structure. *Carbon* **2018**, *140*, 1−9.
(48) Dang, Z.-M.; Jiang, M.-J.; Xie, D.; Yao, S.-H.; Zhang, L.-Q.; Bai, J. Supersensitive linear piezoresistive property in carbon nanotubes/silicone rubber nanocomposites. *J. Appl. Phys.* **2008**, *104*, 024114.
(49) Si, Y.; Yu, J.; Tang, X.; Ge, J.; Ding, B. Ultralight Nanofibre-Assembled Cellular Aerogels with Superelasticity and Multifunctionality. *Nat. Commun.* **2014**, *5*, 5802.
(50) Chen, M.; Li, K.; Cheng, G.; He, K.; Li, W.; Zhang, D.; Li, W.; Feng, Y.; Wei, L.; Li, W.; Zhong, G.; Yang, C. Touchpoint-Tailored Ultrasensitive Piezoresistive Pressure Sensors with a Broad Dynamic Response Range and Low Detection Limit. *ACS Appl. Mater. Interfaces* **2019**, *11*, 2551−2558.
(51) Liu, H.; Dong, M.; Huang, W.; Gao, J.; Dai, K.; Guo, J.; Zheng, G.; Liu, C.; Shen, C.; Guo, Z. Lightweight Conductive Graphene/Thermoplastic Polyurethane Foams with Ultrahigh Compressibility for Piezoresistive Sensing. *J. Mater. Chem. C* **2017**, *5*, 73−83.
(52) Wu, Y.-h.; Liu, H.-z.; Chen, S.; Dong, X.-c.; Wang, P.-p.; Liu, S.-q.; Lin, Y.; Wei, Y.; Liu, L. Channel Crack-Designed Gold@PU Sponge for Highly Elastic Piezoresistive Sensor with Excellent Detectability. *ACS Appl. Mater. Interfaces* **2017**, *9*, 20098−20105.
(53) Liu, H.; Huang, W.; Gao, J.; Dai, K.; Zheng, G.; Liu, C.; Shen, C.; Yan, X.; Guo, J.; Guo, Z. Piezoresistive Behavior of Porous Carbon Nanotube-Thermoplastic Polyurethane Conductive Nanocomposites with Ultrahigh Compressibility. *Appl. Phys. Lett.* **2016**, *108*, 011904.
(54) Ge, J.; Yao, H.-B.; Wang, X.; Ye, Y.-D.; Wang, J.-L.; Wu, Z.-Y.; Liu, J.-W.; Fan, F.-J.; Gao, H.-L.; Zhang, C.-L.; Yu, S.-H. Stretchable Conductors Based on Silver Nanowires: Improved Performance Through A Binary Network Design. *Angew. Chem., Int. Ed.* **2013**, *52*, 1654−1659.

DOI: 10.1021/acsami.9b00900
ACS Appl. Mater. Interfaces 2019, 11, 10922−10932

(55) Li, L.; Zhu, C.; Wu, Y.; Wang, J.; Zhang, T.; Liu, Y. A Conductive Ternary Network of A Highly Stretchable AgNWs/AgNPs Conductor Based on A Polydopamine-Modified Polyurethane Sponge. *RSC Adv.* **2015**, *5*, 62905−62912.
(56) Dong, X.; Wei, Y.; Chen, S.; Lin, Y.; Liu, L.; Li, J. A Linear and Large-Range Pressure Sensor Based on A Graphene/Silver Nanowires Nanobiocomposites Network and A Hierarchical Structural Sponge. *Compos. Sci. Technol.* **2018**, *155*, 108−116.
(57) Kang, D.; Pikhitsa, P. V.; Choi, Y. W.; Lee, C.; Shin, S. S.; Piao, L.; Park, B.; Suh, K.-Y.; Kim, T.-i.; Choi, M. Ultrasensitive Mechanical Crack-Based Sensor Inspired by The Spider Sensory System. *Nature* **2014**, *516*, 222−226.
(58) Fratzl, P.; Barth, F. G. Biomaterial Systems for Mechanosensing and Actuation. *Nature* **2009**, *462*, 442−448.
(59) Yao, H.-B.; Ge, J.; Wang, C.-F.; Wang, X.; Hu, W.; Zheng, Z.-J.; Ni, Y.; Yu, S.-H. A Flexible and Highly Pressure-Sensitive Graphene-Polyurethane Sponge Based on Fractured Microstructure Design. *Adv. Mater.* **2013**, *25*, 6692−6698.
(60) Wicklein, B.; Kocjan, A.; Salazar-Alvarez, G.; Carosio, F.; Camino, G.; Antonietti, M.; Bergström, L. Thermally Insulating and Fire-Retardant Lightweight Anisotropic Foams Based on Nanocellulose and Graphene Oxide. *Nat. Nanotechnol.* **2014**, *10*, 277.
(61) Qian, F.; Lan, P. C.; Freyman, M. C.; Chen, W.; Kou, T.; Olson, T. Y.; Zhu, C.; Worsley, M. A.; Duoss, E. B.; Spadaccini, C. M.; Baumann, T.; Han, T. Y.-J. Ultralight Conductive Silver Nanowire Aerogels. *Nano Lett.* **2017**, *17*, 7171−7176.
(62) Yang, C.; Gu, H.; Lin, W.; Yuen, M. M.; Wong, C. P.; Xiong, M.; Gao, B. Silver Nanowires: From Scalable Synthesis to Recyclable Foldable Electronics. *Adv. Mater.* **2011**, *23*, 3052−3056.
(63) Yang, T. L.; Pan, C. T.; Chen, Y. C.; Lin, L. W.; Wu, I. C.; Hung, K. H.; Lin, Y. R.; Huang, H. L.; Liu, C. F.; Mao, S. W.; Kuo, S. W. Synthesis and Fabrication of Silver Nanowires Embedded in PVP Fibers by Near-Field Electrospinning Process. *Opt. Mater.* **2015**, *39*, 118−124.
(64) Wei, Y.; Chen, S.; Li, F.; Lin, Y.; Zhang, Y.; Liu, L. Highly Stable and Sensitive Paper-Based Bending Sensor Using Silver Nanowires/Layered Double Hydroxides Hybrids. *ACS Appl. Mater. Interfaces* **2015**, *7*, 14182−14191.
(65) Cheng, T.; Zhang, Y.-Z.; Lai, W.-Y.; Chen, Y.; Zeng, W.-J.; Huang, W. High-Performance Stretchable Transparent Electrodes Based on Silver Nanowires Synthesized via An Eco-Friendly Halogen-Free Method. *J. Mater. Chem. C* **2014**, *2*, 10369−10376.
(66) Yang, W.; Li, J.; Zhong, Y.; Qian, H.; Li, Z.; Hu, Y. Facile Cl−-mediated hydrothermal synthesis of large-scale Ag nanowires from AgCl hydrosol. *CrystEngComm* **2013**, *15*, 2598.
(67) Ma, T.; Gao, H. L.; Cong, H. P.; Yao, H. B.; Wu, L.; Yu, Z. Y.; Chen, S. M.; Yu, S. H. A Bioinspired Interface Design for Improving the Strength and Electrical Conductivity of Graphene-Based Fibers. *Adv. Mater.* **2018**, *30*, 1706435.
(68) Ding, Y.; Zhu, J.; Wang, C.; Dai, B.; Li, Y.; Qin, Y.; Xu, F.; Peng, Q.; Yang, Z.; Bai, J.; Cao, W.; Yuan, Y.; Li, Y. Multifunctional Three-Dimensional Graphene Nanoribbons Composite Sponge. *Carbon* **2016**, *104*, 133−140.
(69) Liu, H.; Gao, J.; Huang, W.; Dai, K.; Zheng, G.; Liu, C.; Shen, C.; Yan, X.; Guo, J.; Guo, Z. Electrically Conductive Strain Sensing Polyurethane Nanocomposites with Synergistic Carbon Nanotubes and Graphene Bifillers. *Nanoscale* **2016**, *8*, 12977−12989.
(70) Liu, H.; Huang, W.; Yang, X.; Dai, K.; Zheng, G.; Liu, C.; Shen, C.; Yan, X.; Guo, J.; Guo, Z. Organic vapor sensing behaviors of conductive thermoplastic polyurethane-graphene nanocomposites. *J. Mater. Chem. C* **2016**, *4*, 4459−4469.

DOI: 10.1021/acsami.9b00900
ACS Appl. Mater. Interfaces 2019, 11, 10922−10932